PHYSICAL REVIEW B VOLUME 24, NUMBER 11 1 DECEMBER 1981

Post-field ionization of singly charged rhodium: An experimental and theoretical study

N. Ernst* and Th. Jentsch†
Fritz-Haber-Institut der Max-Planck-Gesellschaft, Faradayweg 4-6, D-1000 Berlin 33, Germany
(Received 29 July 1981)

Differential energy distributions are shown of field-evaporated Rh^+ and Rh^{2+} ions. These spectra have been obtained using a magnetic-sector-field mass spectrometer. Experimental evidence of the occurrence of post-field ionization is presented. This post-field ionization is a process where an initially desorbed Rh^+ ion loses a further electron by ordinary field ionization while traveling away from the rhodium field-emitter surface. The experimental results are compared with calculations using a three-dimensional version of the WKB approximation of the tunneling probability of the valence electron for the desorbing Rh^+ ion. A reasonable agreement between experimental and theoretical data is obtained by including image-force interactions for the tunneling barrier.

I. INTRODUCTION

Field evaporation[1,2] is the process of removing an ion from a field-emitter surface with a high electric field. The field strength is usually between about 20 and 60 V/nm for solid-metal tip emitters. Field evaporation has been frequently used for about thirty years for preparing atomically clean surfaces for field-ion microscopic studies. Two theoretical models have been proposed to explain field evaporation: (a) image hump model[1,2] and (b) charge exchange model.[3–5] Neither model satisfactorily explains the high charge states of field-evaporated ions. To account for these high charge states, post-field ionization of ions, which are initially desorbed in lower charge states, has been considered.[6–9] Calculations of post-ionization probabilities using one-dimensional tunnelling models[10] or transfer Hamiltonian methods[11] have predicted post-ionization as an improbable event. Recent theoretic work by Haydock and Kingham,[12,13] however, suggests that post-ionization may not be as insignificant as previously thought. We will discuss their calculations in more detail in Sec. IV C. Experimental results and conclusions from Ernst[14] on field evaporation of rhodium were supported by Haydock and Kingham's calculations. The statement of Ernst[14] that post-ionization of desorbing Rh^+ ions is the dominant ion generating process for observed Rh^{2+} ions was concluded from three observations: (i) the increase of the relative abundance of Rh^{2+} ions with increasing field strength; (ii) the difference of appearance energies of field-evaporated Rh^+ and Rh^{2+}; and (iii) the equality of activation energies for the two ionic species. These observations provide an indirect test for the post-ionization model but are affected by the inaccuracy in determining the electric field strength. Experimental results of type (i) have also been obtained for Mo and Ir (Ref. 15) and support the post-ionization mechanism for the generation of triply charged ions. Observations of type (i) by Kellogg[16] and by Jentsch and Drachsel[17] and also by Konishi *et al.*[18] do support, furthermore, the occurrence of post-ionization, in particular the possible multiple post-ionization of tungsten ions.[16] Apart from results discussed above there is further direct evidence demonstrating the occurrence of post-ionization. These observations arise from a fourth (iv) class of results that measure the energy distributions of differently charged field-evaporated ions. This has been undertaken by Waugh and Southon[19] as well as by Müller.[20] However, by using a parallel-plate electrostatic energy analyzer without mass-to-charge analysis, Waugh and Southon could not establish the post-ionization mechanism. In this paper experimental results of type (iv) will be reported on the dc field evaporation of Rh^{2+} ions which agree reasonably with calculations based on the post-ionization model. Thus the post-ionization mechanism will finally be established, at least for singly charged rhodium.

II. EXPERIMENT

A. Apparatus

The experimental arrangement has been described previously[21] and consists of the field-ion source, the 60° magnetic sector field (Atlas Mess- und Analysentechnik, GmbH, Bremen, Type: CH4) and the five-electrode energy filter lens[22] as the basic units. Slight modifications have been performed within the field-

ion source. As can be seen in Fig. 1, ions, which are generated at the tip-emitter surface, are focussed onto the entrance slit of the magnetic mass spectrometer by means of a three-electrode lens, similar to that used in connection with a quadrupole mass spectrometer.[23] Rhodium-tip emitters have been spot-welded onto a molybdenum supporting wire and could be cooled to approximately liquid-nitrogen temperature. The whole experimental arrangement including an open secondary electron multiplier (SEM) is mounted within a bakable and differentially pumped ultrahigh vacuum chamber with a typical base pressure in the lower 10^{-10} Torr range. The tip emitter was heated by applying an ac voltage across the Mo wire. The temperature of the emitter was measured using an iron constantan thermocouple. Rhodium-tip emitter surfaces were cleaned by heating and field evaporation. The cleanliness of the surfaces was determined by means of field-electron images which could be viewed on the luminescent screen of the counter electrode through a window, indicated by the arrow in Fig. 1. With the use of the present ion optics the most favorable distance between probe hole and tip-emitter surface for detection of maximum ion counting rates was smaller than 2 mm. Therefore, no face-specific measurements have been performed. Differential energy distributions were measured by sweeping the tip potential with the magnetic field strength held constant (Figs. 2 and 3). This is, in principle, the same method as previously applied for field-ionized gases by Jason[24] and Hanson.[25]

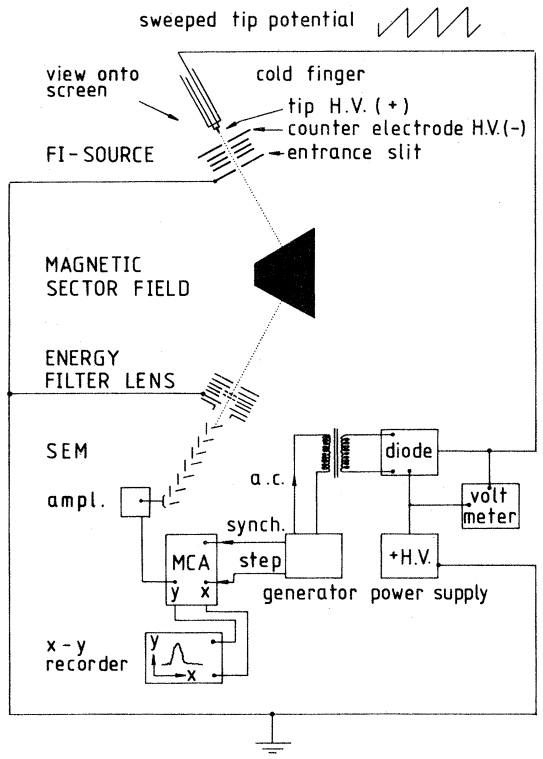

FIG. 1. The experimental arrangement consists of a vacuum chamber, which contains the field-ion source, the magnetic sector field, and the energy filter lens as the basic units. Ions, which have passed the energy filter lens, are detected by a secondary electron multiplier (SEM). Ion signals are stored on the y axis of a multichannel analyzer (MCA), whose x axis is swept by an external generator. Thus, differential energy distributions of field evaporated ions may be displayed on the cathode ray tube of the MCA.

B. Results

Experimental conditions have been judiciously chosen so that field-evaporated singly as well as dou-

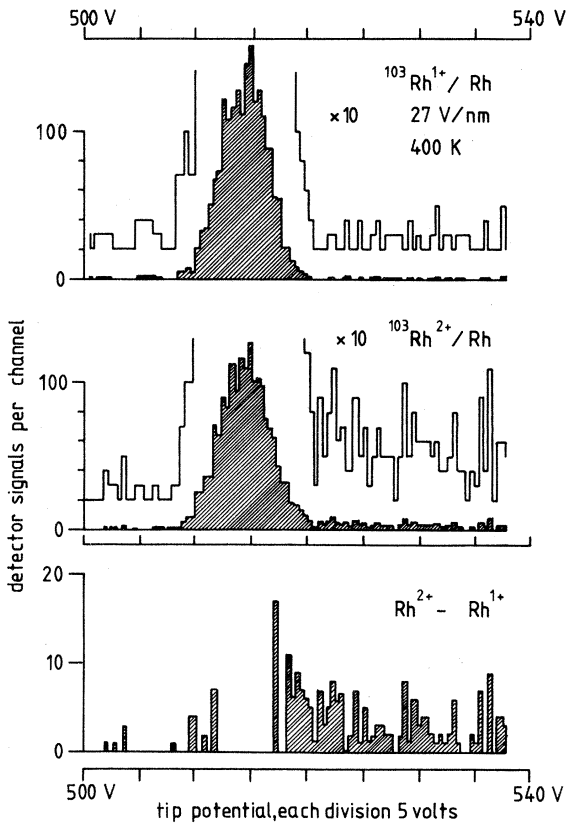

FIG. 2. Differential energy distributions of field-evaporated singly and doubly charged rhodium ions measured with an overall electric field strength of about 27 V/nm (tip-counter electrode voltage: 17.0–20.3 kV) and an emitter temperature of 400 K (upper two diagrams). The lower diagram displays the difference of the Rh^{2+} and the Rh^{1+} spectra (negative values omitted). Rh^{2+} ions of low kinetic energy are detected on the right-hand side of the Rh^{2+} main peak. Low-energy ions are not observed for field-evaporated Rh^{1+}.

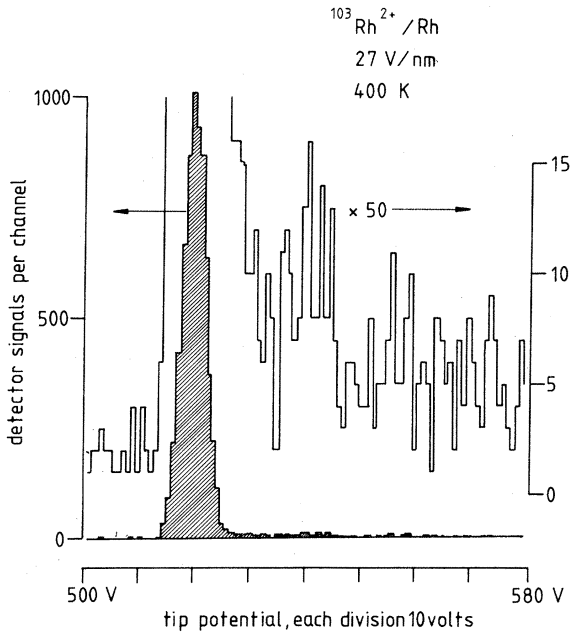

FIG. 3. Energy distribution of field-evaporated Rh^{2+} demonstrating the tailing of low-energy ions down to about 100 eV beyond the main peak position (160 eV full scale, tip-counter electrode voltage: 7.5–26.4 kV).

bly charged species could both be measured. With an overall field strength value of 27 V/nm derived from FN plots of the field-electron current (accuracy about ±15%) both ionic species Rh^+ and Rh^{2+} evaporate with nearly equal abundance as previously reported.[14] For the present experiments the tip-emitter temperature was adjusted to 400 K in order to obtain reasonable ion counting rates and, consequently reasonable signal-to-noise ratios for energy distribution measurements. The thermally induced diffusion of rhodium surface atom occurring at this temperature[26] is not of importance in the post-ionization of a desorbing ion which is the concern of this paper.

With the use of the present ion optics we could achieve an energy resolution of 4 eV, full width at half maximum (FWHM) for singly charged species and an ion counting rate of about five counts per second for experimental conditions as shown in Figs. 2 and 3. As can be clearly seen from the spectra of field-evaporated Rh^{2+} ions, there is a tailing to decreasing kinetic energy in contrast to Rh^+ ions. This finding is in excellent agreement with the formerly proposed post-ionization mechanism for the field evaporation of Rh^{2+} (Ref. 14) and will be discussed in Sec. III. The low kinetic energy tail of the Rh^{2+} ion energy distribution could be suppressed by means of the energy filter lens[27] so that any kind of ion-optical artifact could be excluded.

III. THE POST-IONIZATION MODEL

A schematic diagram illustrating the process of post-field ionization is given in Fig. 4. Post-ionization of initially desorbed one fold charged ions can only occur at distances greater than the minimum distance x_p^{min}. This is similar to the ordinary case of field ionization of neutrals.[6] It is only here that the energy levels of the valence electrons (upper left part of Fig. 4) are elevated due to the external field F by such an amount that tunnelling into empty electronic states at and above the Fermi energy E_F becomes possible. Ionization can also occur at larger distances where no appreciable surface effect exists (free-space ionization).

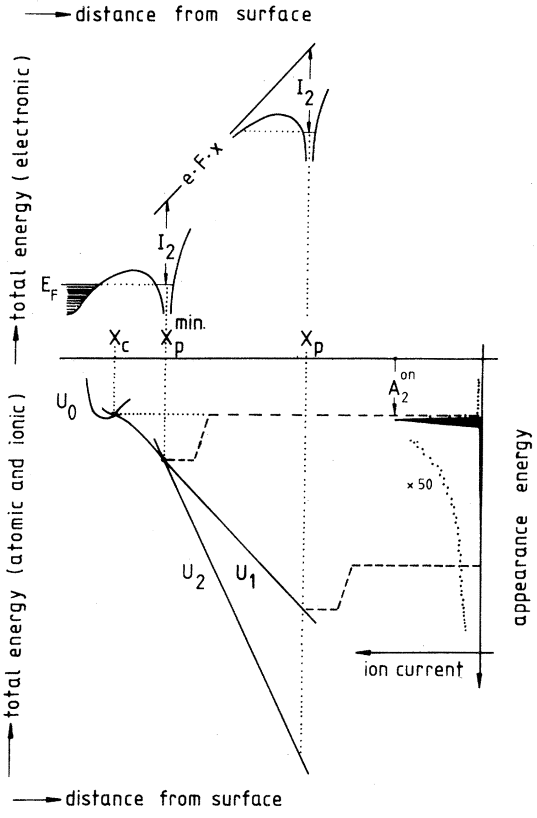

FIG. 4. Schematic diagram of the post-ionization model of field evaporation. In the upper left part of the figure are shown potential energy curves for the valence electrons of Rh^{1+} ions which are located at distance x_p^{min} and x_p from the field-emitter surface, respectively. The lower left drawing, a so-called Gomer-Swanson diagram (Refs. 28 and 29), displays potential energy curves of the neutral U_0, and of Rh^{1+} and Rh^{2+} ions, U_1 and U_2, respectively. On the right-hand side is schematically shown the differential energy distribution as measured for field-evaporated Rh^{2+}. The onset appearance energy A_2^{on} of the energy distribution is a measure for the point of potential energy $U_1(x_c)$ of initially desorbed Rh^{1+} ions, which are post-field ionized at the minimum distance x_p^{min}.

The lower left part of Fig. 4 displays a graph of the total (atomic and ionic) energy versus distance from the emitter surface. U_0, U_1, and U_2 represent the potential energies of the neutral, singly and doubly charged atoms, respectively. A singly charged ion starting at distance x_c gains kinetic energy while travelling along curve U_1. At $x_p^{\min}$ it is possible that the ion becomes post-ionized and its potential energy is then given by curve U_2. The appearance energy A_2^{pn} as depicted in the right diagram is mainly determined by the point of potential energy $U_1(x_c)$, the starting-point potential energy of the singly charged ion. Detailed mechanisms of the initial evaporation step at x_c have been generally discussed by Forbes[7,29,30] and by Ernst[14] as well as by Ernst and Block[31] for the field evaporation of rhodium. These mechanisms are of little importance in the calculation of post-ionization probabilities as performed in Sec. IV. A singly charged ion which is post-ionized at a relatively large distance, say x_p, displays a larger deficit in kinetic energy or larger appearance energy value than ions which are post-ionized at the minimum distance $x_p^{\min}$. Measurements of appearance energies thus provide a means for determining the site of post-ionization.[27]

IV. CALCULATION OF POST-IONIZATION PROBABILITIES FOR SINGLY CHARGED IONS

A. Model

The tunneling probability is calculated in terms of the WKB approximation, using a potential barrier generated by the applied field, the charge of the ion, and the image charges of the ion and the electron. By integration over the angle with respect to field direction (as in Ref. 13), a three-dimensional tunneling probability is obtained, and by multiplication with an electronic frequency factor ν with which the electron strikes the barrier, and by taking the velocity of the accelerated ion into account, the probability of post-ionization is evaluated as a function of field strength and the distance from the surface.

The tunnelling potential for the electron (compare with Fig. 5) is given by

$$V(x,r,\Theta) = -\frac{2}{r} + \frac{2}{r_i} - \frac{1}{4(x - r\cos\Theta)} - Fr\cos\Theta \tag{1}$$

for the post-ionization of a singly charged ion, x being the distance of the ion from the surface, r the distance of the electron from the ion core, Θ the angle with respect to the external electric field F, and r_i the distance of the electron from the image of the ion, which is given by

$$r_i = [(r\sin\Theta)^2 + (2x - r\cos\Theta)^2]^{1/2} \ . \tag{2}$$

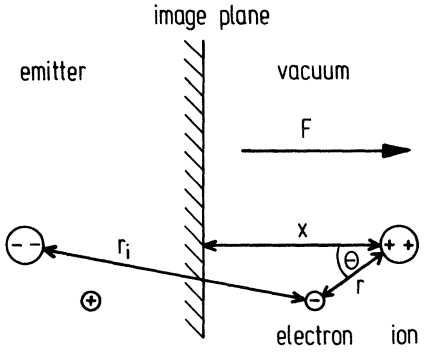

FIG. 5. Charge distribution for the calculation of the tunneling potential.

All expressions are in atomic units ($\hbar = m = e = 1$). The first term in Eq. (1) accounts for the potential of the ion core, the second one for its image potential, the third one for the image potential of the tunneling electron, while the last one is the electron's energy in the external field. Variation of field strength as a function of distance from the tip surface and tip radius r_{tip} is taken into account by setting

$$F = F_0 \frac{r_{\text{tip}}}{r_{\text{tip}} + 2(x - r\cos\Theta)} \ , \tag{3}$$

with F_0 being the field strength at the surface, assuming the tip to be of paraboloid shape.[11,32]

The one-dimensional tunneling probability for the electron in the WKB approximation is then given by

$$T_{1D}(x,\Theta) = \exp\left[-8^{1/2}\int_{r_1}^{r_2}[\,V(x,r,\Theta) - E(x)]^{1/2}\,dr\right] \ , \tag{4}$$

r_1 and r_2 being the zeros of the integrand and $E(x)$, the total energy of the electron, being

$$E(x) = -I_2 + \frac{3}{4x} \ . \tag{5}$$

In Eq. (5) I_2 is the second ionization energy and the last term the difference in image potential energies of the singly and doubly charged ions. Other contributions, such as Stark shift or field penetration, are ignored for the present calculations.

In a next step, a three-dimensional tunnelling probability is obtained as in Ref. 13 by integration over the azimuthal and polar angles

$$T_{3D}(x) = \alpha 2\pi \int_{\theta=0}^{\pi/2} T_{1D}(\Theta,x)\sin\Theta\, d\Theta \ , \tag{6}$$

The factor 2π results from integration over the azimuthal angle and α is a constant in the order of one accounting for the inexactness of this kind of approximation.

The local ionization rate I of an ion stationary at x is then obtained by multiplication with the electronic frequency factor ν

$$I(x) = \nu T_{3D}(x) \quad . \tag{7}$$

The probability density for the ion to be ionized at x passing this point x with a velocity $v(x)$ is then

$$\rho(x) = I(x) v(x)^{-1} \quad . \tag{8}$$

Post-ionization leads to a reduction of singly charged ions available for post-ionization at larger distances. The probability for a desorbing ion to be post-ionized along its way to a point at a distance z from the surface is then given by

$$P(z) = 1 - \exp\left[- \int_{x_p^{\min}}^{z} \rho(x)\, dx \right] \quad . \tag{9}$$

No post-ionization is possible for distances smaller than $x_p^{\min}$, which is approximately given by

$$F x_p^{\min} = I_2 - \phi \quad , \tag{10}$$

since at this point the electron's energy equals the lowest free state available for tunnelling in the metal (see Fig. 4). In Eq. (10) ϕ is the work function of the emitter. The probability density for an ion leaving the surface to be post-ionized at $x = z$ is

$$\rho^*(z) = [1 - P(z)]\rho(z) \quad , \tag{11}$$

since only a fraction $[1 - P(z)]$ of ions reaches this point in a singly charged state. ρ^* is the quantity to be compared with the experimentally observed energy distribution of the doubly charged ions.

For simplicity in calculation, the initial evaporation of the singly charged ion is described by a classical image hump process[2,6] and $v(x)$ was calculated accordingly. This is sufficiently exact for present purposes. More realistic assumptions, as inferred from appearance energy data,[14] lead to lower values of $v(x)$ and thus slightly higher value of ρ^* near to the surface.

For the determination of a numerical value for ν, a simple Bohr orbital picture was used. A value of the order of $\nu = 10^{15}\ \mathrm{s}^{-1}$ for the post-ionization of singly charged rhodium was estimated.

B. Calculations

The calculation was carried out numerically using an integration method of the Romberg type with an error of one part in 10^{-3} in each dimension. The angle of integration was limited to $\Theta = 50°$, since tunnelling at larger angles does not contribute significantly. This was established by test runs using larger angles.

Figure 6 shows the experimental results of Ernst[14]

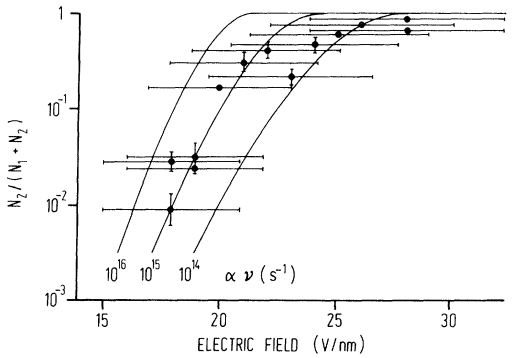

FIG. 6. Probability of post-ionization of Rh^+ as a function of field strength. Experimentally determined ratio $N_2/(N_1+N_2)$ (current of Rh^{2+} to total ion current) is taken from Ernst (Ref. 14). Calculations were performed for three different values of $\alpha\nu$ and $r_{tip} = 100$ nm.

for the field dependence of post-ionization probability of rhodium and the results of the numerical calculations using three different values of $\alpha\nu$, which is the only unsufficiently known factor in the model. As can be seen, the theory fits reasonably well for the value $\alpha\nu = 10^{15}\ \mathrm{s}^{-1}$ obtained from the Bohr picture, though the experimentally observed field strengths seem to be slightly higher than those predicted by the calculations. Integration over the distance from the surface was carried out up to $z = 4x_p^{\min}$, because in the measurements of Ernst[14] ions with large energy deficits were not taken into account. At intermediate field strengths and with $r_{tip} = 100$ nm, as used in the present calculation, about 10% of the total amount of doubly charged ions are expected with higher energy deficits.

Figure 7 is a plot of the probability density for post-ionization ρ^* calculated according to Eq. (11), as a function of the distance from the surface for six different field strengths. A value $\alpha\nu = 1 \times 10^{15}\ \mathrm{s}^{-1}$ and $r_{tip} = 100$ nm was used. The maximum of the post-ionization probability is found at $x = x_p^{\min}$, where a sharp cutoff due to the Pauli principle exists. The steep increase of ρ^* near $x_p^{\min}$ is due to surface effects, in particular the sharp cutoff of the tunnelling barrier. The decrease at larger distances is essentially caused by a decrease in field strength, the reduction of ions available for post-ionization, and an increase in velocity of the particles. The ratio of the peak height at $x_p^{\min}$ to the values of ρ^* at larger distances decreases from low to intermediate field strengths. There is a maximum of ions originating at larger distances at a field strength of about 22 V/nm, which roughly corresponds to an overall post-ionization probability of 50%. Increasing the field strength further leads to a pronounced decrease of intensity at larger distances, since most of the ions have already been ionized nearer to the surface.

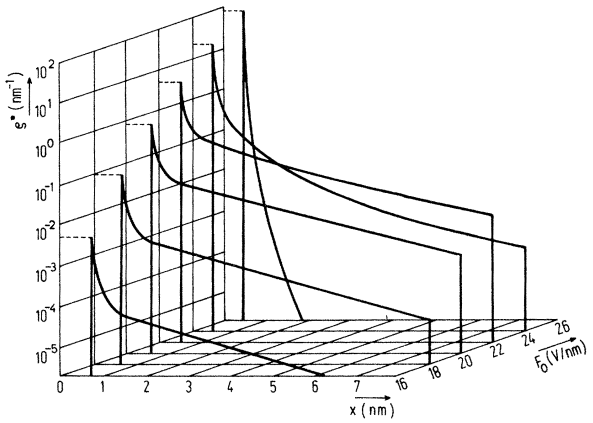

FIG. 7. Theoretical prediction for the probability density ρ^* of post-ionization of Rh^+ as a function of the field strength F_0 at the surface and the distance x from the surface. Calculations were done with $\alpha\nu = 10^{15}\ s^{-1}$ and $r_{tip} = 100$ nm.

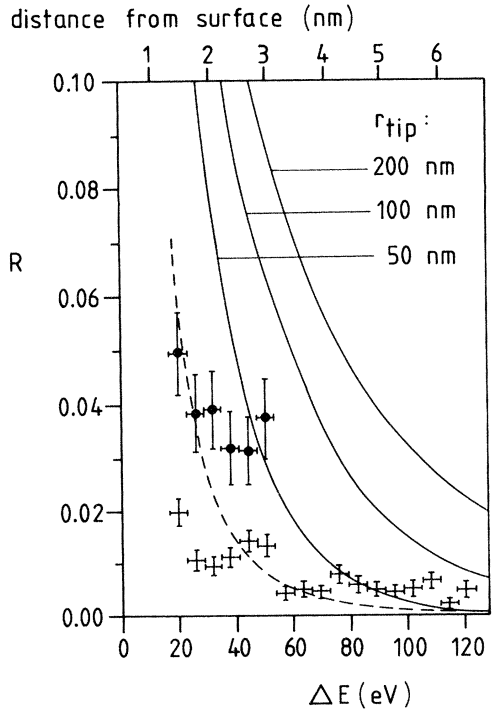

FIG. 8. Comparison of experimentally determined relative abundances R of Rh^{2+} ions with theoretical predictions as a function of the energy deficit ΔE. The solid lines have been calculated for three different tip radii r_{tip} and for $F_0 = 22$ V/nm. The dashed line has been calculated for $r_{tip} = 100$ nm and for $F_0 = 24$ V/nm ($\alpha\nu = 10^{15}\ s^{-1}$). Data points have been derived from the experiments of Fig. 2 (⊕) and of Fig. 3 (+), respectively. The calculation of R and the conversion of the energy scale into the distance scale are explained in the text. For the dashed line, only the energy scale applies.

In order to compare the experimentally observed energy distribution with the calculation, one must allow for the broadening of the peak structure due to the limited resolution of the apparatus. To this end, we calculated the ratio R of the probability density ρ^* at point x beyond the main peak position to the mean $\bar{\rho}^*$ in a region Δx_0 at x_p^{min}

$$R(x) = \frac{\rho^*(x)}{\bar{\rho}^*_{\Delta x_0}} \quad . \tag{12}$$

By making the region of averaging Δx_0 broad enough to include totally the experimentally broadened main peak, the obtained ratio $R(x)$ becomes independent of the resolution of the apparatus.

To convert the energy scale of the experiment to the distance scale of the calculation, the field strength used in the calculation ($F_0 = 22$ V/nm and $F_0 = 24$ V/nm, respectively) was assumed to apply also for the experimental situation. In order to account for the asymmetric energy distribution, the distance x_p^{min}, with a corresponding energy deficit $\Delta E = 0$ eV (by definition), was assigned to an energetic position lying 3.2 eV to the left from the main peak position in Fig. 3. Ignoring this shift results in changes of less than 10% in the values of R to be compared. The mean of ρ^* was taken over a region of a width of 16 eV for the experimental data and a corresponding length extending from x_p^{min} to $x_p^{min} + 0.73$ nm for the calculation ($F_0 = 22$ V/nm, $x_p^{min} = 0.6$ nm).

For comparison Fig. 8 shows values of R derived from two different experiments with different tips and those derived from calculations. The theoretical curves were calculated for $F_0 = 22$ V/nm (and a corresponding post-ionization probability $P \approx 50\%$), using three different tip radii (solid lines), and for $F_0 = 24$ V/nm ($P \approx 90\%$) and $r_{tip} = 100$ nm (dashed line). A value $\alpha\nu = 10^{15}\ s^{-1}$ was used throughout.

The theory fits the experimental data reasonably well, especially if one bears in mind that there is a maximum of the calculated tailing at $F_0 \approx 22$ V/nm ($P \approx 50\%$). The overestimation of the tailing by the theory for this field strength may be partly explained by the fact that it was not possible to achieve a constant 50% post-ionization probability experimentally. (The tip radii have been estimated to be about 100 nm or more). There is a large scatter in the experimental results. The differences between the two experiments are probably due to different tip radii, since the experimental points in the upper part of Fig. 8 correspond to the experiment of Fig. 2. Here (⊕), the experiment has been performed by using a tip emitter which, on the average, had a greater radius than in the experiment of Fig. 3 (+).

C. Comparison with previous calculations

Previous calculations using one-dimensional tunnelling methods[10] or transfer Hamiltonian methods[11] led to the conclusion that post-ionization is a negligible effect. Experimental work by Ernst[14] provided evidence for post-ionization of rhodium ions, and he fitted his data with a calculation using a one-dimensional tunnelling formalism over a simple triangular potential barrier.[6] In a recent theory, Haydock and Kingham constructed a three-dimensional tunnelling probability using the WKB approximation identical to the present calculation, but instead of using the physically justifiable tunneling potential, Eq. (1), they used a simple model potential for ease in calculation, and fitted their theory to the experimental data by choosing an appropriate value of the effective charge number of the ion which is thought to include effects of the image potentials. Their paper[13] contains an error, since by applying the charge numbers stated in it, the potential barrier breaks down well below field strengths stated to correspond to a post-ionization probability of 10%.[33] In a subsequent paper[34] based on the same theory, they predict an energy distribution for doubly charged rhodium which displays a less pronounced tailing effect than our experiments.

In a recent paper, Konishi *et al.*[18] calculate the post-ionization probability for gallium, again using the WKB approximation and a tunneling potential similar to ours. Instead of constructing a three-dimensional tunneling probability by integration over the angles, they correct their one-dimensional results by a method described by Müller and Bahadur.[35] Neglection of the image term in their formula for the electron's total energy [as done in Eq. (5) in this work], while using image terms for the potential energy of the tunneling electron, should lead to a decrease of ρ^* at $x_p^{\min}$ and to the appearance of a second maximum of ρ^* at larger distances from the surface and thus to an overestimation of the tailing.

V. CONCLUSION

We have attempted to demonstrate both experimentally and theoretically that field evaporation of Rh^{2+} ions occurs via a two-stage process. First there is initial evaporation as Rh^+ and this is followed by post-field ionization of desorbing Rh^+. The observation of low-energy Rh^{2+} ions provides direct experimental evidence for the post-ionization mechanism. Plasmon effects, formerly discussed by Lucas,[36] may be excluded in the explanation of present experimental results. This is because field-desorbed Ne^{2+} ions did not display a low kinetic energy tail.[37] A "Jason" structure[24,34] within the energy distribution of Rh^{2+} ions due to resonances involved in the electron tunnelling process could not be established experimentally because of limited energy resolution.

The number and the residence time of Rh^+ ions which pass the post-ionization zone may be determined experimentally. This allows us to derive a value for the free-space field-ionization rate I for Rh^+ of the order of 10^{11} s^{-1} from present experimental results ($F \approx 25$ V/nm). This value is somewhat smaller than our calculated value using the WKB approximation. The magnitude of our experimental value of I seems to be quite reasonable in comparison to other calculated values of the Stark ionization rate of hydrogen atoms.[38,39] These calculations obtain values for I which are greater by about one order of magnitude (10^{12} s^{-1}, $F = 25$ V/nm) than our experimental value of I for Rh^+. This is in accordance with the fact that compared to Rh^+ the ionization energy of H is smaller by an amount of 4.4 eV. Further experiments of the type as presented above could yield more data on ionization rates in high electric fields, in particular the dependence on field strength. Furthermore, the post-ionization mechanism for generation of triply and quadruply charged ions remains to be verified by direct experimental observations.

In conclusion, the present study finally solves the longstanding controversy on the probability of post-field ionization, at least for singly charged ions and thus gives a contribution to a better understanding of field-evaporation and field-desorption processes.

ACKNOWLEDGMENTS

We gratefully acknowledge the excellent technical assistance of Mr. G. Bozdech. We are indebted to Professor J. H. Block for his continuous interest in this work.

*Author to whom inquiries should be sent.

†Calculations in Sec. IV have been performed in partial fulfillment of the Dr. rer. nat. degree of the Freie Universität, Berlin.

[1] E. W. Müller, Naturwissenschaften 29, 533 (1941).

[2] E. W. Müller, Phys. Rev. 102, 518 (1956).

[3] T. T. Tsong and E. W. Müller, Phys. Status Solidi A 1, 513 (1970).

[4]T. T. Tsong, J. Chem. Phys. 54, 4205 (1971).
[5]T. T. Tsong, Surface Sci. 70, 211 (1978), and references therein.
[6]E. W. Müller and T. T. Tsong, Prog. Surface Sci. 4, 1 (1973).
[7]R. G. Forbes. Surf. Sci. 61, 221 (1976).
[8]S. Nakamura and T. Kuroda, Jpn. J. Appl. Phys. 16, 1499 (1977).
[9]N. Ernst, G. Bozdech, and J. H. Block, Surf. Sci. 80, 645 (1979).
[10]D. M. Taylor, Ph. D. thesis (University of Cambridge, 1970) (unpublished).
[11]R. S. Chambers, University of Illinois Report No. R 1702, 1975.
[12]R. Haydock and D. R. Kingham, J. Phys. B 14, 385 (1981).
[13]R. Haydock and D. R. Kingham, Phys. Rev. Lett. 44, 1520 (1980).
[14]N. Ernst, Surf. Sci. 87, 469 (1979).
[15]N. Ernst and G. Bozdech, in *Proceedings of the 27th International Field Emission Symposium,* edited by Y. Yashiro and N. Igata (University of Tokyo, Tokyo, 1980), p. 100.
[16]G. L. Kellogg, Phys. Rev. B (in press).
[17]Th. Jentsch and W. Drachsel (unpublished).
[18]M. Konishi, M. Wada, and O. Nishikawa, Surf. Sci. 107, 63 (1981).
[19]A. R. Waugh and M. J. Southon, J. Phys. D 9, 1017 (1976).
[20]E. W. Müller, Ber. Bunsenges. Phys. Chem. 75, 979 (1971).
[21]N. Ernst, G. Bozdech, and J. H. Block, Int. J. Mass Spectrom. Ion Phys. 28, 33 (1978).
[22]N. Ernst, Dissertation (Freie Universität Berlin, 1976) (unpublished).
[23]A. Martin and J. H. Block, Messtechnik (Braunsehweig) 5, 155 (1973).
[24]A. J. Jason, Phys. Rev. 156, 266 (1967).
[25]G. R. Hanson, J. Chem. Phys. 62, 1161 (1975).
[26]G. L. Kellogg and T. T. Tsong, J. Appl. Phys. 51, 1184 (1980); G. L. Kellogg, Ultramicroscopy 5, 260 (1980).
[27]N. Ernst and G. Bozdech, in *Proceedings of the 28th International Field Emission Symposium,* edited by L. W. Swanson and A. Bell (The Oregon Graduate Center, Beaverton, 1981), p. 32.
[28]R. Gomer and L. W. Swanson, J. Chem. Phys. 38, 1613 (1963).
[29]R. G. Forbes, Prog. Surf. Sci. (in press).
[30]R. G. Forbes, Surface Sci. 70, 239 (1978); 102, 255 (1981).
[31]N. Ernst and J. H. Block, Surface Sci. 91, L27 (1980).
[32]H. D. Beckey, H. Krone, and F. W. Röllgen, J. Phys. E 1, 118 (1968).
[33]D. R. Kingham (unpublished).
[34]R. Haydock and D. R. Kingham, Surf. Sci. 104, L194 (1981).
[35]E. W. Müller and K. Bahadur, Phys. Rev. 102, 624 (1956).
[36]A. A. Lucas, Phys. Rev. Lett. 26, 813 (1971).
[37]N. Ernst, Phys. Rev. Lett. 45, 1573 (1980); N. Ernst and J. H. Block, in *Proceedings of the 28th International Field Emission Symposium,* edited by L. W. Swanson and A. Bell (The Oregon Graduate Center, Beaverton, 1981), p. 41.
[38]H. J. Silverstone, B. G. Adams, J. Cizek, and P. Otto, Phys. Rev. Lett. 43, 1498 (1979).
[39]L. Benassi and V. Grecchi, J. Phys. B 13, 911 (1980).